AD-A069 151 INDIANA UNIV AT BLOOMINGTON DEPT OF CHEMISTRY F/G 7/4
EXPERIMENTAL STUDIES ON SPATIAL DISTRIBUTIONS OF ATOMS SURROUND--ETC(U)
MAY 79 C B BOSS, G M HIEFTJE N00014-76-C-0838
UNCLASSIFIED TR-26 NL

| OF |
AD
A069151

END
DATE
FILMED
6-79
DDC

AD A069151

DDC FILE COPY

UNCLASSIFIED
SECURITY CLASSIFICATION OF THIS PAGE (When Data Entered)

(12)

REPORT DOCUMENTATION PAGE

READ INSTRUCTIONS BEFORE COMPLETING FORM

1. REPORT NUMBER: TWENTY
2. GOVT ACCESSION NO.
3. RECIPIENT'S CATALOG NUMBER

4. TITLE (and Subtitle): (6) Experimental Studies on Spatial Distributions of Atoms Surrounding an Individual Solute Particle Vaporizing in an Analytical Flame,
5. TYPE OF REPORT & PERIOD COVERED: (9) Interim Technical Report,
6. PERFORMING ORG. REPORT NUMBER: 26

7. AUTHOR(s): (10) C. B. Boss and G. M. Hieftje
8. CONTRACT OR GRANT NUMBER(s): N00014-76-C-0838

9. PERFORMING ORGANIZATION NAME AND ADDRESS: Department of Chemistry, Indiana University, Bloomington, IN 47405 (11) 25 May 79
10. PROGRAM ELEMENT, PROJECT, TASK AREA & WORK UNIT NUMBERS: NR 051-622

11. CONTROLLING OFFICE NAME AND ADDRESS: Office of Naval Research, Washington, D. C.
12. REPORT DATE: May 25, 1979
13. NUMBER OF PAGES: 39

14. MONITORING AGENCY NAME & ADDRESS (if different from Controlling Office): (12) 44 p.
15. SECURITY CLASS. (of this report): UNCLASSIFIED
15a. DECLASSIFICATION/DOWNGRADING SCHEDULE

LEVEL II

16. DISTRIBUTION STATEMENT (of this Report)

Approved for public release; distribution unlimited

(14) TR-26, 20

17. DISTRIBUTION STATEMENT (of the abstract entered in Block 20, if different from Report)

(15) N00014-76-C-0838

DDC RECEIVED MAY 30 1979 C

18. SUPPLEMENTARY NOTES

Prepared for publication in Analytical Chemistry

19. KEY WORDS (Continue on reverse side if necessary and identify by block number)

atomic absorption, multielement analysis, interelement interferences, particle vaporization, atomic diffusion

20. ABSTRACT (Continue on reverse side if necessary and identify by block number)

An experimental procedure is described which allows the direct, time-resolved investigation of the spatial distribution of analyte atoms surrounding an individual solute particle vaporizing in a laminar flame. In the procedure, the individual atomic clouds are observed spectrometrically as the flame sweeps them past a fixed horizontal viewing region. The spatial intensity profiles so obtained are treated by a spherically symmetric Abel-type series, to provide the radial analyte distribution in each cloud. These measured radial distri-

DD FORM 1 JAN 73 1473 EDITION OF 1 NOV 65 IS OBSOLETE S/N 0102-014-6601

UNCLASSIFIED
SECURITY CLASSIFICATION OF THIS PAGE (When Date

176 685

79 05 29 06

bution in each cloud. These measured radial distributions are used to experimentally verify a theoretical model, previously described, which convolves the processes of analyte vaporization and diffusion. From measured vaporization rates and least-squares fits to experimental data, effective diffusion coefficients for analyte atoms are determined. The lateral diffusion interference of phosphate on calcium in nitrous oxide-acetylene flames is also studied with the new method. It was found that the calcium vaporization rate and not its diffusion coefficient changes with addition of phosphate, causing the observed alteration in spatial distribution.

OFFICE OF NAVAL RESEARCH

Contract N00014-76-C-0838

Task No. NR 051-622

TECHNICAL REPORT NO. 20

EXPERIMENTAL STUDIES ON SPATIAL DISTRIBUTIONS OF ATOMS SURROUNDING AN INDIVIDUAL SOLUTE PARTICLE VAPORIZING IN AN ANALYTICAL FLAME

by

C. B. Boss and G. M. Hieftje

Prepared for Publication

in

ANALYTICAL CHEMISTRY

Indiana University

Department of Chemistry

Bloomington, Indiana 47405

May, 1979

ABSTRACT

An experimental procedure is described which allows the direct, time-resolved investigation of the spatial distribution of analyte atoms surrounding an individual solute particle vaporizing in a laminar flame. In the procedure, the individual atomic clouds are observed spectrometrically as the flame sweeps them past a fixed horizontal viewing region. The spatial intensity profiles so obtained are treated by a spherically symmetric Abel-type series, to provide the radial analyte distribution in each cloud. These measured radial distributions are used to experimentally verify a theoretical model, previously described, which convolves the processes of analyte vaporization and diffusion. From measured vaporization rates and least-squares fits to experimental data, effective diffusion coefficients for analyte atoms are determined. The lateral diffusion interference of phosphate on calcium in nitrous oxide-acetylene flames is also studied with the new method. It was found that the calcium vaporization rate and not its diffusion coefficient changes with addition of phosphate, causing the observed alteration in spatial distribution.

BRIEF

An experimental method is described which allows the measurement of solute vaporization rates and atomic diffusion coefficients. A reduced vaporization rate is shown to be the cause of the lateral diffusion interference of phosphate on calcium in N_2O/C_2H_2 flames.

Both chemical flames and inductively coupled radio-frequency plasmas have proven to be excellent atom reservoirs for use in atomic spectrometric analysis. In both these sources, an aerosol of sample solution must be vaporized to produce the atoms needed for measurement in the ultra-violet and visible regions. As each of the aerosol species vaporizes, its gaseous products move away and ultimately merge with those from neighboring particles to yield a more or less spatially continuous sample for spectrometric measurement. It is important that this vaporization and vapor-phase homogenization occur as completely as possible. For example, if liberated analyte atoms should migrate only a short distance from vaporizing solute particles in a flame or plasma, the individually produced clouds of atomic vapor would not overlap; as these atom-rich regions consecutively pass the source viewing region, a great deal of flicker noise would appear in the spectrometric signal (1) and adversely affect both analyte detectability and measurement precision.

A related problem concerns measurement errors which arise from changes in the lateral distribution of atoms in the flame or plasma as a consequence of sample matrix variations. Koirtyohann and Picket (2) measured the lateral distribution of atoms in a N_2O/C_2H_2 flame supported on a slot burner and found not only that the atom concentration was much greater in the center of the flame but also that the atomic spatial distribution changed from sample to sample, leading to a possible interference. West, Fassel, and Kniseley (3) further studied the phenomenon, labeling it a "lateral diffusion interference" and proposed that it arose from a shift in the maximum region of solute vaporization.

There are many plausible mechanisms for these "lateral diffusion interferences". L'vov (4) contends that they are caused in some cases by a change in the lateral distribution of aerosol droplets as they emerge

from the burner top. The droplets roughly follow the flame gases as they expand at and immediately behind the flame front. The amount of lateral force applied to a particular droplet then depends on the droplet's diameter, mass, and orientation as it leaves the burner top. Thus, any change in the sample matrix which significantly alters the density of the solution or the size of the nebulized aerosol droplets might cause a lateral diffusion interference.

Another possible mechanism for this interference suggests that vaporized matrix components change the flame's chemistry in the region where analyte volatilizes. Such a change could cause the equilibrium between free elemental species and molecules to shift. In turn, the predominant analyte-carrying species would differ in the immediate vicinity of the vaporizing particle. Because the newly predominant species (say molecules) would be unlikely to have the same vapor-phase mobility as the original ones (say atoms and ions), the ultimate lateral distribution of analyte atoms would be different, and an interference would be observed.

A third possible mechanism for the lateral diffusion interference involves the rate of analyte volatilization directly, as suggested by West, et al. (3). Changes in analyte volatility do more than move the free atom distribution up and down in the flame. In a preceding paper (5), it was shown theoretically that changes in analyte vaporization can cause variations in the shape of the vapor cloud created by the vaporization of a single, isolated aerosol particle. Thus, differences in analyte volatility can affect atom distribution in a manner similar to that of diffusion rate and thereby produce a lateral "diffusion" interference.

Distinguishing experimentally between these three mechanisms in any particular situation will require a detailed understanding of the factors which affect the spatial distribution of atoms vaporized from an individual

solute particle in an analytical flame. An experimental technique will be described here which enables this understanding to be obtained. The technique is based on photometric observation of the atoms in a thin horizontal region of the flame as an individual vaporizing solute particle is swept vertically through it by the rising flame gases. By photometrically scanning the particle and its surrounding vapor cloud vertically rather than horizontally, the new technique enjoys instrumental simplicity and freedom from flame edge effects.

The results of these investigations confirm that a previously reported theory (5) can successfully predict the spatial distribution of analyte atoms liberated in the flame. This fit between theory and experiment not only validates the theory but also provides a means of measurement of the effective diffusion coefficient of analyte in the flame. Unlike some other diffusion coefficient measurement techniques (6), the new approach employs the natural spherical symmetry of diffusion from individual aerosol particles.

The agreement between the results obtained herein and the behavior predicted theoretically (5) enables the contributions of diffusion and particle vaporization to "lateral diffusion interference" to be understood. In particular, the lateral diffusion interference of phosphate on calcium in a laminar N_2O/C_2H_2 flame is found to be caused by slowed calcium volatilization; the calcium diffusion coefficient remains essentially constant upon addition of phosphate to the matrix.

EXPERIMENTAL

To study the time-resolved spatial distribution of atoms in detail, the sample introduction technique of Hieftje and Malmstadt (7) has been employed. In this approach, uniform-sized sample droplets are reproducibly injected into

a laminar analytical flame to yield a spatial and temporal resolution of the processes occurring to the droplet and its condensed and vapor-phase products. Because the flame drives the injected aerosol particles and their products upward with a uniform velocity (7,8), the vertical distance in the flame provides a convenient time scale for monitoring the various events and determining their rates. This resolution makes it possible to monitor the changing spatial distribution of atoms in a spherical cloud of vapor surrounding a single solute particle. It is only necessary to observe, by absorption, emission, or fluorescence, the concentration profile of atoms in the cloud as they sweep by a chosen viewing region; in the present study, emission from the atoms was employed. By moving the observation region up and down in the flame, it is then possible to quantitatively determine the temporal behavior of the vapor cloud.

Flames and Burners. For the air-acetylene flame used in these studies, the burner and gas supply systems have been previously described (9). The rise velocities of air-acetylene flames supported on this burner have been characterized by an atomic vapor cloud velocity measurement technique (9). The flow rates of 2.7 L/min acetylene, 18 L/min air, and 3.25 L/min sheathing N_2 used for the present studies yield a flame with a measured rise velocity of 9.3 m/s.

For the nitrous oxide-acetylene flame, the burner top was changed to one with 0.45 mm diameter holes arranged in a pattern similar to that in the air-acetylene top. Nitrous oxide was regulated and metered in equipment identical to that used for air. Flows of 3.0 L/min acetylene, 13.8 L/min nitrous oxide, and 2.0 L/min sheathing nitrogen produced the stable, laminar flame used in these experiments. The rise velocity of this nitrous oxide-acetylene flame was also measured with the atomic vapor cloud technique (9) and found to be 15.3 m/s.

Sample Introduction System. The device used to repetitively introduce uniform-sized droplets of sample solution into flames is similar in design to those described in previous studies (7,9,10). Figure 1 shows a schematic representation of this droplet generator and associated measurement optics. The uniform droplets are produced by forcing the analyte solution through a capillary whose end is constricted to a diameter of 20 to 40 μm depending upon the droplet size desired. The liquid jet formed at the end of the capillary is then caused to disintegrate into droplets by vibrating the capillary with a piezoelectric ceramic bimorph (Clevite Corporation, Bedford, OH) driven at a frequency between 25 and 60 kHz by an osciallator (Model 200CRD, Hewlett Packard Corporation, Palo Alto, CA). The diameters of droplets produced by the generator were measured prior to each experiment by observing stroboscopically illuminated droplets through a microscope fitted with a calibrated reticle. To ensure that atomic vapor clouds do not overlap in the flame, the droplet introduction rate must be reduced to 500 Hz or lower. This frequency division is accomplished by charging certain droplets and removing them from the droplet stream. A voltage pulse on a cylindrical electrode surrounding the liquid jet serves to charge the droplet that breaks from the jet while the pulse is being applied. This charged droplet will then be deflected when it travels through a strong externally established electric field, will miss a trap stationed to catch the main (uncharged) droplet stream, and will enter the flame.

Measurement of Analyte Vapor Cloud Profiles. For the observation and measurement of atom vapor cloud concentration profiles, the experimental arrangement of Figure 1 was employed. In this system, a monochromator (Model EU-700, GCA McPherson Instrument Company, Acton, MA) was tilted 90° from its usual orientation so its entrance and exit slits were horizontal

rather than vertical, and could therefore provide improved vertical spatial resolution. While this tilting caused the sine bar drive in the monochromator to track less accurately than in the normal position, the stability of a fixed wavelength setting did not appear to be degraded, as evidenced by the constancy of the monitored signal from an atomic line empirically centered in the slit.

With this modification, a dove prism is no longer required for image rotation (7), alignment is easier, and the light lost from prism surfaces is eliminated. A single condensing lens can now be used to focus the flame onto the monochromator's entrance slit, making the slit a spatial filter imaged within the flame. Back-illumination of this optical system through the monochromator indicates that the region in the flame from which emitted light is detected approximates a horizontal disk. To assure that the viewing region covers the entire width of the flame, the lens is situated to provide an optical magnification of -0.25 of the flame onto the monochromator's entrance slit. The vertical thickness of this viewing region is in fact controlled by the monochromator slit width and by this optical magnification. Most measurements were made with a slit width of 100 μm which translates into a 0.4 mm thickness of the viewing region in the flame.

The output of the photomultiplier is amplified by a photometric preamp (Model 221, Princeton Applied Research Corporation, Princeton, NJ) and transmitted to the analog input of a PDP 12/40 mini-computer (Digital Equipment Corporation, Maynard, MA). Data conversion at the computer's maximum rate, measured to be 19.6 μs per point, provides adequate temporal resolution of the observed signals, which range in duration from approximately 100 μs to greater than 5 ms.

Signal Extraction. The noise that exists on the detected signal is often large enough to require some signal enhancement. Because the shape of the signal carries desired information about the radial concentration of analyte in the vapor cloud, distortion cannot be tolerated and simple analog filtering techniques (11) cannot be used. Instead, only signal enhancement techniques which do not distort the shape of the signal, such as boxcar integration and signal averaging, can be used. Unfortunately, these techniques require an accurate timing signal which this droplet generation system does not readily supply. The charging pulse which the droplet generator uses to select droplets might seem to be such a trigger; however, the small droplets used in this technique are strongly affected by air currents outside the flame and by turbulence at the flame boundary, making very poor the synchronization between the charging pulse and the movement of the corresponding droplet. Of course, a trigger signal could be derived from the vaporization of the droplet contents themselves. For example, such a trigger has been produced (12) by doping the sample matrix with a highly emissive element such as potassium, and by detecting the start of emission of that element when particle vaporization begins. Unfortunately, such an approach requires addition of a foreign synchronizing element to the sample solution, and will probably produce different condensed or vapor-phase behavior of the analyte, a consequence that cannot be tolerated here.

To overcome these obstacles, a new kind of self-triggered signal averaging algorithm was developed. Although the new method is of limited utility under conditions of very poor signal-to-noise ratio, it performs well in the present application. Basically, the algorithm overcomes a signal time jitter by sensing the signal's initiation and termination and centering the signal within an appropriate time window. Summation of all signal replicas in the same window then provides the necessary temporal registration

to produce signal-to-noise improvement. The new signal enhancement algorithm was software configured and integrated into the data collection routines. A flow chart of the resulting program is given in Figure 2. As revealed in Figure 2, the signal is sampled and digitized for 80 ms and the resulting data are searched for peaks which represent the passage of an atomic vapor cloud. Each digitized peak is then centered and summed into a signal averaging buffer to accomplish the required signal-to-noise enhancement. During the initialization phase of the program, several parameters such as data storage location in memory, signal threshold level, and the size of the signal-averaging window are entered through the computer terminal. After this initial phase, the control of data collection, signal averaging, and storage is transferred to a three-push-button control panel located at the experimental apparatus. Depressing a buttom marked DATA on the panel causes the computer to acquire 4096 data points at the maximum analog input rate. These data are searched for the peaks that occur when a vapor cloud image passes the slit.

Each peak is detected in the digitized data array by a positive-slope threshold crossing followed by a negative-slope crossing. This use of two threshold crossings to center the peak within the signal averaging window effectively eliminates centering errors caused by noise on the data (under the signal-to-noise conditions employed in this study), compared to single threshold crossing techniques. With this approach, the selected threshold value is relatively unimportant and can be varied from 20% to 80% of the total peak height with no apparent effect on the signal averaging process. Combined with a moderate amount of digital smoothing (used only to find the threshold crossings and not present in the final averaged data) this technique centers peaks within 10 μs of the true center of the window. This

error is the least allowed by the digital sampling of the waveform, so the final averaged signal should faithfully represent the true waveform.

After these operations are complete, the average data peak is displayed on a monitor stationed at the experimental apparatus and the operator can choose among several ways to proceed. One choice is to collect another 4096 data points and average the newly detected peaks with the buffer, thereby increasing the degree of noise reduction. A second choice is to reject the newly displayed data and start the data collection-signal averaging process again. A third option that the operator can choose is to store the data on magnetic tape. The data collection and signal averaging sections of this program require less than one second to complete while the storage of data on magnetic tape requires between two and three seconds.

For each averaged peak obtained through the above procedure, a manual measurement is made to determine the temporal location of that particular signal with respect to the beginning of particle vaporization. The measurement simply involves determining the distance between the lowest point where analyte emission can be observed in the flame and where the photometric system is imaged. Both these locations are ascertained by means of a cathetometer. The image point of the entrance slit in the flame is found by back illumination of the optical system; the start of analyte emission is a well-defined point at the bottom of the visible vapor clouds. This distance measurement can be related to time through knowledge of the flame's rise velocity.

Reagents. Solutions of Ca salts were prepared from dried, reagent-grade $CaCO_3$ and concentrated reagent-grade acids HNO_3 and HCl. Phosphate was added as H_3PO_4, pipetted from a stock solution titrated against NaOH, which in turn was standardized with dried, primary standard grade potassium hydrogen phthalate. Solutions of NaCl were prepared from the reagent-grade salt. Stock solutions were generally prepared at the 10,000 µg/mL level.

RESULTS AND DISCUSSION

Characteristics of the Observed Signal. A typical signal peak is shown in Figure 3; from such a signal, the spatial distribution of atoms vaporized from an individual solute particle can be determined. The signal in Figure 3 was recorded from a vapor cloud formed after the desolvation and vaporization of an 80 μm aerosol droplet containing 100 μg/mL sodium as NaCl. The shape, width and area of this signal all convey important information concerning the vapor cloud.

The area under the observed signal is proportional to the total number of atoms in the vapor cloud. Because each atom in the cloud spends approximately the same length of time in the monochromator's viewing region, each will statistically emit the same number of photons in the viewing direction. In order to symbolically differentiate between this peak area and the original signal-averaged peaks, let $i(t)$ be the time-resolved, signal-averaged photocurrent and $I(t)$ be the area under the curves $i(t)$, where the time reference t for the areas is measured from the beginning of analyte emission to the passage of the center of the vapor cloud through the imaging region. The fact that $I(t)$ represents the number of atoms present in the vapor cloud at a particular time can be experimentally substantiated: $I(t)$ measured at the completion of analyte vaporization for uniform droplets containing different concentrations of sodium increases linearly with concentration over the range of 10 to 200 μg/mL.

The shape of the signal peak, $i(t)$, contains information about the radial distribution of analyte atoms in the vapor cloud. Clearly, a larger vapor cloud will produce a broader signal peak, and a more diffuse cloud will generate a lower, wider peak, because of the constant velocity at which each cloud passes through the viewing region. However, more subtle features in

the peak shape are significant and a detailed, albeit qualitative analysis of the shape is justified. Upon close observation, it can be seen that the leading and trailing edges of the peak in Figure 3 have different slopes. This finding can be explained by the diffusion which the cloud undergoes as it passes through the viewing region. As the cloud enters the viewing region, it is relatively compact and its concentration gradient consequently steep. Thus, the photomultiplier signal rises rapidly from the background and reaches a maximum as the center of the vapor cloud passes the viewing region. This maximum occurs not only because the center of the cloud has a higher atom concentration than the cloud extremities, but also because the cloud's thickness is greatest when viewed through its center.

As the cloud traverses the slit image, diffusion serves to spread the cloud, so that it is larger when leaving the region than when it entered. The consequently lowered concentration gradient in the more diffuse cloud causes the trailing edge of the peak to have a lower slope than did the leading edge. Thus, the signal has imbedded in it even information concerning the variation of radial concentration profile which occurs within the vapor cloud over the period of observation. Of course, a detailed comparison between these experimentally observed data and the theory of spatial distributions (5) requires a quantitative relationship between the radial atomic concentrations and the observed signal. Such a relationship can be derived through application of an Abel inversion (13,14).

Spherical Abel-type Series. The quantitative relationship between the radial atomic concentrations and the observed signal is a spherical Abel-type integrator series. The true Abel series is a construction in forming the Abel transform (13,14) which, in turn, allows radially dependent functions to be derived from measurements made on a cylindrically symmetric system. In a similar treatment, to be developed here, a spherical rather than cylindrical

Abel-type series is employed to determine radial atom concentrations from measurements taken through an entire cross-section of a spherical atom cloud. Simply viewed, the new algorithm inverts the process of mathematically summing the number of atoms present in the intersection of the viewing region and atom cloud. Thus, the inversion mathematically strips away the contributions of spherically symmetrical shells in the vapor cloud, rather like peeling an onion.

Let $C(r,t)$ be the concentration of analyte atoms at a distance r from the center of the vapor cloud and at a time t, measured from the start of analyte vaporization. The intersection between the viewing region and the spherically symmetric vapor cloud is schematically represented in Figure 4. Let R be the vertical distance from the center of mass of the analyte vapor cloud to the plane which horizontally defines the viewing region. Let ΔR be the height of the viewing region. The central volume of this construction is dome-shaped and bounded by the plane which crosses the z-axis at $R - 1/2\Delta R$ and by the sphere of radius $R + 1/2\Delta R$. The volume of this central dome is:

$$V_O = \frac{\pi(\Delta R)^2}{3}(3R + \Delta R) \qquad (1)$$

The remaining sections of this slice of the vapor cloud are a series of annular regions bounded on the top and bottom by the planes $z = R + \Delta R/2$ and $z = R - \Delta R/2$ and on their sides by the spheres $r = R + (n - 1/2)\Delta R$ and $r = R + (n + 1/2)\Delta R$ where n is the shell number and ranges from +1 to $+\infty$. The volume of the nth region is:

$$V_n = \pi(\Delta R)^2[R(2n + 1) + R(n^2 + n + 1/6)] \qquad (2)$$

The total number of atoms in the viewing region may now be obtained as the product of the volume and concentration in each region summed over the entire viewing volume:

$$N(t) = C(R,t)\ V_o + \sum_{n=1}^{\infty} C(R + n\Delta R, t)\ V_n \qquad (3)$$

Because the instantaneous atomic emission measurement is proportional to the total number of atoms in the viewing volume, the observed signal $\underline{i(t)}$ is proportional to $\underline{N(t)}$ in equation 3.

In principle, it is possible to invert these equations to obtain a function proportional to $\underline{C(r,t)}$ (the desired quantity) from an experimentally observed signal, $\underline{i(t)}$. However, because vaporization and diffusive transport of analyte occur significantly during the observation time, this inversion is mathematically complicated and requires a knowledge of the form of the function $\underline{C(r,t)}$. A more reasonable approach to take, in the comparison of theory to data, is to use the theoretically derived expressions for $\underline{C(r,t)}$ in equation 3 and fit the resulting function to the data.

A theoretically based expression for the temporal and radial distribution of atoms in an atomic vapor cloud has been shown to be (5):

$$C(r,t) = \frac{q}{4\pi rD}\left[\left(t + \frac{Q}{q} + \frac{r^2}{2D}\right)\operatorname{erfc}\left(\frac{r}{2(Dt)^{1/2}}\right) - r\left(\frac{t}{\pi D}\right)^{1/2} e^{-r^2/4Dt}\right] \qquad (4a)$$

$$\text{for } 0 \le t \le t_f$$

and

$$C(r,t) = \frac{q}{4\pi rD}\left(\left[t + \frac{Q}{q} + \frac{r^2}{2D}\right]\left[\operatorname{erfc}\left(\frac{r}{2(Dt)^{1/2}}\right) - \operatorname{erfc}\left(\frac{r}{2[D(t-t_f)]^{1/2}}\right)\right] + \frac{r}{(\pi D)^{1/2}}\left[(t-t_f)^{1/2}\, e^{-r^2/4D(t-t_f)} - t^{1/2}\, e^{-r^2/4Dt}\right]\right)$$

$$\text{for } t > t_f \qquad (4b)$$

where D is the diffusion coefficient, and t represents the time after the onset of analyte vaporization. The parameters q, Q, and t_f originate from a linear approximation of the analyte vaporization function:

$$\Phi(t) = qt + Q \qquad \text{for } 0 \leq t \leq t_f \qquad (5)$$

where $\Phi(t)$ is the rate of release of analyte atoms (atom/s). This representation of the atomic concentration has been shown to correspond very well to the atomic concentrations predicted by the theoretically rigorous convolution of measured vaporization rate and diffusion (5). It remains to find experimental values for q and Q in equation 5, an endeavor quite straightforward with the present apparatus.

Analysis of the Spatial Distribution of Ca in an Air-Acetylene Flame. The spatial distribution of Ca atoms in various analytical flames has been experimentally studied by several investigators (6,15,16). Because of the volume of these available independent but similar experimental data, calcium was selected as the element for investigation in the present work as well. Specifically, the radially and temporally dependent concentration of calcium atoms in the spherical vapor cloud produced by an individual, vaporizing $CaCl_2$ particle in an air-acetylene flame was measured and compared with the previously derived theory represented by equation 4.

Individual particles were produced for examination by injecting into a fuel-rich air-acetylene flame 58 μm diameter droplets containing 100 μg/mL Ca as $CaCl_2$. The vapor cloud profiles, $\underline{i(t)}$, for the Ca atoms, observed at the 422.7 nm Ca line, were recorded at several points in the history of the vapor cloud development; a plot of the area $\underline{I(t)}$, of these curves as a function of time in their development is shown in Figure 5 and is essentially the impulse response function (10) of the flame. Bastiaans and Hieftje (10) have demonstrated that the shape of the leading edge of a plot such as Figure 5 is determined by the volatilization rate of analyte atoms. Thus, the leading edge of the flame's impulse response function should be approximated by the integral of equation 5, namely:

$$I(t) = qt^2/2 + Qt \qquad \text{for } t \leq -Q/q \qquad (6)$$

A regression analysis fit of equation 6 to the observed data (Figure 5) yields the impulse response function denoted by the solid line in Figure 5 and the expression:

$$I(t) = 1.03 \times 10^9\ t^2 + 1.22 \times 10^6\ t \qquad \text{for } t < 1.18 \times 10^{-3}\ s \qquad (7)$$

Now that the parameters in equation 4 dealing with the vaporization of analyte have been defined for these calcium particles in an air-acetylene flame, the radial distribution of atoms can be compared to theory. In particular, the shape of the data curves $\underline{i(t)}$ resulting from individual vapor clouds passing the viewing region of the optical system can be compared to the model involving convolution between vaporization and diffusion to predict the spatial distribution of atoms. To begin, the spherical

Abel-type series, equation 3, relates $C(r,t)$ of the theory to the data curves obtained, $i(t)$. Next, cathetometer measurements, combined with the measured flame velocity give directly the time between the start of analyte vaporization and the passage of the center of the atomic vapor cloud through the viewing region. It remains to determine which point in the data array corresponds to the time (t_1) at which the center of the vapor cloud passes the viewing region. This factor (t_1), the effective diffusion coefficient of the analyte, D, and a proportionality factor, m, are all found by fitting the theoretical curve to the experimental data. The factor m simply reflects a proportionality between the number of analyte atoms in the viewing region, $N(t)$, and the observed data. It combines many constants which affect the data, including the fraction of atoms which emit, the optical speed of the collection-dispersion system, and the electronic gain. The fitting is performed by non-linear least-squares regression analysis (17). An example of the fit between the theoretical and experimentally observed curves is shown in Figure 3.

The fit between theory and experiment displayed here is a good indication that the theory adequately (within experimental error) represents the spatial distribution of atoms from an individual solute particle. This thesis is further substantiated through an examination of the adjustable parameters used to fit the theory of experiment. Data for the spatial distribution of Ca were taken between 0.5 ms and 2.3 ms after the initiation of Ca vaporization. Over this entire range, when theory and experimental data are fit, t_1 occurs very close to the center of the signal averager window and m varies according to the electronic gain as expected.

Of even greater interest are the diffusion coefficients, D, found for the best fits, which are plotted against time from the onset of vaporization in Figure 6. Close to the start of Ca vaporization (left part of Figure 6),

the calculated D value is large and not very precise, while at longer times, D is fairly constant at 3.4 cm^2/s. This behavior is understandable, since small errors in the cathetometer measurements used to establish t_o and t will be relatively larger at short times than at long times and will affect the calculated diffusion coefficients correspondingly. Also, the linear volatilization theory used here and developed in a preceding paper (5) has been shown to be most accurate after vaporization is complete. Thus, the final value of D observed in Figure 6 can be considered most accurate and agrees well with values for the diffusion coefficient of Ca in an air-acetylene flame (3 to 5 cm^2/s) reported by Snelleman (6). The fact that these three adjustable parameters are consistent is a good indication that the spatial distribution of analyte atoms from individual solute particles can be reliably predicted by the convolution of vaporization and diffusion when the linear-vaporization model is employed.

Measurement of the Diffusion Coefficients of Na in an Air-Acetylene Flame. In a similar experiment to the one described above, the diffusion coefficient of sodium in an air-acetylene flame was measured and produced a value of $D = 12.3 \pm 0.2$ cm^2/s. This compares favorably to the value of 9.9 ± 5 cm^2/s obtained by Snelleman (6) under similar conditions.

This method for the measurement of diffusion coefficients in flames offers several advantages over previously used techniques. First, the theory takes account of the effect vaporization has on the spatial distribution of atoms. The natural spherical symmetry of diffusion from a point source is preserved throughout. Also, diffusion into the edges of the flame does not greatly influence the findings of this measurement technique. Third, the situation occurring in conventional analytical flames is closely simulated, making it easier to investigate the interaction of diffusion with other condensed- and vapor-phase processes in determining overall atom

distributions. The importance of this latter fact is underscored in the following section.

Mechanism for Lateral Diffusion Interference of Phosphate on Calcium in a N_2O/C_2H_2 Flame. It is well documented that the phosphate anion severely depresses atomic spectrometric signals for elemental calcium in air-acetylene flames by trapping the calcium in arefractory matrix, thereby inhibiting the Ca volatilization (18). This interference can be reduced either by matrix modification, i.e., incorporating a high concentration of a releasing agent such as lanthanum in the solution, or by using hotter flames, like N_2O/C_2H_2, to more rapidly vaporize the refractory matrix. The latter technique reduces the interference to a few percent and some investigators have even noticed an enhancement of Ca signals due to phosphate in the matrix. West, Fassel, and Kniseley (16) determined that Ca atoms released in N_2O/C_2H_2 flames from solutions containing phosphate migrate toward the edges of the flame more slowly than do those from phosphate-free solutions. No mechanism has yet been proven for this "lateral diffusion" interference, although these previous workers (16) tentatively ascribed the effect to slowed particle volatilization.

In a previous paper (5), a theoretical model was used to show that a more compact vapor cloud formed by the volatilization of an individual solute particle can be attributed either to changes in the diffusion coefficient or to changes in the vaporization rate. It is conceivable that either factor could be the cause of the "lateral diffusion" effect and it is important to experimentally verify or refute the suggested mechanism (16). The experimental methods detailed in this paper provide a method for distinguishing between effects induced by vapor phase mobility changes and vaporization rate changes. In such a study, uniform droplets (65 μm diameter) of either aqueous $CaCl_2$ or aqueous $H_3PO_4/CaCl_2$ (each containing 100 μg Ca/mL)

were injected into a fuel-rich N_2O/C_2H_2 flame at a rate of approximately 400 droplets/s. Alkemade and Voorhuis (18) have shown that the maximum effect of the vaporization interference of phosphate on calcium occurs at a P/Ca molar ratio greater than 0.4. Accordingly, P/Ca molar ratios used here were 0.0 0.5, and 1.0. No detectable differences were found between the effect of 0.5 and 1.0 P/Ca ratios so that only the 0.5 P/Ca case will be discussed below.

First, it is essential to determine that phosphate addition does not significantly alter the nature of the processes leading to particle vaporization. In an earlier study (10) it was shown that desolvation can be affected at high solute concentration by a fragmentation of solute material. Such fragmentation was accompanied by an earlier appearance (lower in the flame) of atomic vapor emission, and this earlier emission can be used to test the existence of the effect.

In the experimental system used herein, the flame drives the pertinent condensed and vapor phase species at its own rise velocity (after the initial droplet acceleration period), so the time which elapses between sample introduction and first analyte emission can readily be measured from the distance between the vertical location where droplets are introduced and where analyte emission is first observed. When this difference was measured, the droplets containing phosphate required approximately 0.65 ms longer to produce atomic vapor than did phosphate-free droplets, this time representing a relative change of approximately 5%. This measured small change is probable due to the extra time required for the solute particles containing phosphate to reach the higher temperature they require to begin vaporizing (7) and indicates an absence of solute fragmentation.

This change in position where vaporization begins is probably not significant in the interference suffered in conventional atomic absorption experi-

ments. First, most of the desolvation in such systems likely occurs before the sample actually enters the flame or within the first centimeter of the flame (19). Second, the primary reaction zone of the flame heats the particles very quickly in conventional systems, reducing small relative changes in heating times. While this process might be responsible for some of the observed upward movement of the maximum calcium spectrometric signal when phosphate is present, it is undoubtedly overshadowed by the increased time the particle with phosphate takes to vaporize.

The overall volatilization history of Ca from particles comprised of these two matrices is strikingly different; Figure 7 compares the vaporization profiles [I(t)] of the two. In Figure 7, the time origin (t = 0) represents the start of analyte emission. Phosphate-free calcium, it is seen, vaporizes faster than does a particle having a phosphate matrix; furthermore, the phosphate-free calcium signal reaches a high level before ionization decreases it (10). The plateau reached by both signals in Figure 7 indicates complete vaporization of the respective particle (10), and a consequently equal area of the recorded signal i(t). However, although the areas of the i(t) curves are equal, their shapes differ greatly, reflecting the distinct shapes of the corresponding vapor clouds. Figure 8 shows the signals observed when calcium vapor clouds, one from a completely volatilized phosphate-containing and one from a volatilized phosphate-free matrix, pass the experimental viewing region 4.0 ms after the start of emission. Clearly, the signal produced by the vapor cloud from the phosphate-free calcium particle is broader, indicating a more diffuse cloud. Because the vapor clouds are scanned vertically in this technique, this finding suggests that "lateral diffusion" affects the individual vapor clouds isotropically, thus obviating the need to invoke mechanisms involving flame edge effects.

In addition to the above qualitative results, these data provide the

information necessary to decipher the relative roles of the diffusion coefficient and vaporization rate in generating more compact calcium atom clouds from solute particles having a phosphate matrix. Fitting the two impulse response functions of Figure 7 to equation 6 shows that the vaporization rate of calcium with phosphate is 30% slower than that of the phosphate-free calcium. Further fitting of the original data curves, $\underline{i(t)}$, to equation 4 reveals that the diffusion coefficients are essentially equal for the two matrices at a value of 10.8 ± 0.2 cm^2/s. This compares well with the value of 9.3 cm^2/s measured by Joshi (20) for calcium in a N_2O/C_2H_2 flame.

In the flames used by Koirtyohann (2) and West (3) it was conceivable that changes in either analyte diffusion coefficients or vaporization rates caused the calcium atoms to remain closer to the center of the flame when phosphate was added to the matrix. This ambiguity in the interference mechanism has been resolved by the experiment reported above. Because only the rate of vaporization of calcium, and not its diffusion coefficient, was found to change with the addition of phosphate to the matrix, the vaporization rate change must be the cause of the more compact vapor clouds observed.

CONCLUSIONS

A model for the spatial distribution of analyte atoms formed by vaporization of an individual particle in a laminar flame presented earlier (5) is confirmed by experimentally observed behavior. The theory, as used here, incorporates a linear approximation to the analyte vaporization function and convolves this behavior with analyte diffusion. The resulting function, equation 4, can be fit to data which represent the shape of the atomic vapor cloud. The success of this fit shows that not only the diffusion coefficient, but also the vaporization rate can be important factors in determining the shape of atomic vapor clouds and the distribution of analyte atoms in a flame.

Several consequences of these findings to practical flame spectrometry arise and accrue from the importance of the shape and breadth of the individually produced atomic vapor clouds in such a system. One factor which is strongly affected is analyte flicker noise, which limits both sensitivity and precision in practical flame methods (1). If analyte atoms diffuse away from vaporizing particles rapidly, to produce an almost uniform analyte concentration in the flame, the flicker caused by a particle drifting into or out of the spectrometric viewing region will be small. In contrast, if analyte vaporization yields dense, compact vapor clouds, the entry or exit of such a cloud will cause considerable signal flicker.

Another problem which is directly related to the spatial distribution of atoms liberated from an individual solute particle is the lateral spread of atoms in the flame. Changes in this spread have been identified as a source of an interference (2, 3). Obviously, a sample and standard must produce the same distribution of analyte if accurate calibration is to be assured.

Because the spatial distribution of analyte is an important factor in determining an atomic spectrometric signal, these distributions must be included in attempts to use atomic spectrometry as an absolute measurement method. Efforts to achieve absolute atomic spectrometry (21,22) are primarily aimed at a detailed mathematical description of the measurement systems presently in use. While a detailed mathematical description of these systems will not soon replace standards and working curves in atomic spectrometry, a detailed knowledge of the effects of various parameters on an atomic system will help the analyst intelligently find optimal conditions for a particular analysis. The inclusion of the atomic spatial distributions surrounding individual vaporizing solute particles, theoretically described earlier (5) and experimentally confirmed here, is important in

properly describing lateral migration of atoms and analyte flicker noise in flame spectrometry.

LITERATURE CITED

1. N. W. Bower and J. D. Ingle, Jr., Anal. Chem., 49, 574 (1977).
2. S. R. Koirtyohann and E. E. Pickett, Anal. Chem., 40, 2068 (1968).
3. A. C. West, V. A. Fassel, and R. N. Kniseley, Anal. Chem., 45, 1586 (1973).
4. B. V. L'vov, L. P. Kruglikova, L. K. Polzik, and D. A. Katskov, J. Anal. Chem. USSR, 30, 545 (1975).
5. C. B. Boss and G. M. Hieftje, Anal. Chem., (in press, 1979).
6. W. Snelleman, Ph.D. Thesis, Univ. of Utrecht, 1965.
7. G. M. Hieftje and H. V. Malmstadt, Anal. Chem., 40, 1860 (1968).
8. C. B. Boss and G. M. Hieftje, Anal. Chem., 49, 2112 (1977).
9. C. B. Boss and G. M. Hieftje, Appl. Spectrosc., 32, 337 (1978).
10. G. J. Bastiaans and G. M. Hieftje, Anal. Chem., 46, 901 (1974).
11. K. R. Betty and G. Horlick, Appl. Spectrosc., 30, 23 (1976).
12. R. L. Cochran and G. M. Hieftje, Anal. Chem., 49, 98 (1977).
13. A. Scheeline and J. P. Walters, Anal. Chem., 48, 1519 (1976).
14. R. N. Bracewell, Aust. J. Phys., 9, 198 (1956).
15. C. Th. J. Alkemade, Ph.D. Thesis, Univ. of Utrecht, 1954.
16. A. C. West, V. A. Fassel, and R. N. Kniseley, Anal. Chem., 45, 2420 (1973).
17. B. M. Shchigolev, Mathematical Analysis of Observation, American Elsevier Publishing Co. Inc., New York, N.Y. (1965).
18. C. Th. J. Alkemade and M. H. Voorhuis, Fresenius' Z. Anal. Chem., 163, 91 (1958).
19. J. B. Willis, Spectrochim. Acta, Part A, 23, 811 (1967).
20. B. M. Joshi, Ph.D. Thesis, Univ. of Michigan, 1977.
21. B. V. L'vov, D. A. Katshov, L. P. Kruglikova, and L. K. Polzik, Spectrochim. Acta, Part B, 31, 49 (1975).
22. K.-P. Li, Anal. Chem., 48, 2050 (1976).

GLOSSARY OF TERMS

$C(r,t)$	the concentration of analyte atoms at a distance r from the center of the vapor cloud at time t.
D	Fick's law diffusion coefficient.
$I(t)$	the intensity of analyte atomic line radiation emitted from the entire vapor cloud at time t after vaporization begins.
$i(t)$	the intensity of analyte atomic line radiation emitted in the spectrometer viewing region at time t.
$N(t)$	the number of atoms in the viewing volume.
Q	rate of analyte vaporization at time t = 0 in the linear approximation to the analyte vaporization rate (cf. Ref. 5).
q	the slope of the linear approximation to the vaporization rate (cf. Ref. 5
R	the vertical distance from the center of mass of the analyte vapor cloud to the plane which horizontally defines the spectrometer viewing region
r	distance from the center of mass of the atomic vapor cloud to a point in the vapor cloud.
ΔR	the height of the viewing region.
t	time measured from the beginning of analyte vaporization.
t_f	the completion time of analyte vaporization in the linear approximation.
V_n	the volume of the nth ring in the spherical Abel series.
$\Phi(t)$	the rate of release of analyte atoms at time t.

CREDIT

Supported in part by the National Science Foundation through grant CHE 77-22152 and by the Public Health Service through grant GM 17904-06.

FIGURE CAPTIONS

Figure 1. Apparatus used to measure the spatial profiles of individual emitting atomic vapor clouds. Uniform droplets are injected into a laminar analytical flame with a droplet generator similar to that of Hieftje and Malmstadt (7). The spherical clouds of atomic vapor produced by vaporization of analyte from the individual droplets are swept through the viewing region by the rising flame gases. The viewing region in the flame is defined by the image of the horizontal entrance slit of the monochromator. The shape of the resulting signal carries information about both the radial distribution of atoms in the spherical cloud and the total number of vapor-phase atoms in the cloud.

Figure 2. Block diagram of self-triggered software signal averager. Program acquires 4096 data points and searches data for peaks. Each discovered peak is centered and summed into the SUM buffer. The SUM buffer is then divided, point by point, by the number of peaks found to form a single signal-averaged peak. Push-buttom (PB) control then enables the data to be stored, rejected or averaged with a new set of raw data for further signal-to-noise enhancement (see text for further explanation).

Figure 3. Typical signal cuased by an individual vapor cloud passing the viewing region in the flame. In this figure, the averaged signal from 33 droplets, .80 μm in diameter and each containing 100 μg Ca/ml, vaporizing in an air-acetylene flame, is shown as individual data points. The solid line in this figure represents the fit of equation 4 to these data. In producing the fit, a value for the calcium diffusion coefficient (D) of 3.42 cm^2/s was found.

Figure 4. Construction used for the spherical Abel-type series. The series sums the atoms in a thin planar viewing region from a spherical vapor cloud. The thickness of the viewing region is defined as ΔR and the distance from the center of the vapor cloud to the center of the viewing region is R. The volume of the dome-shaped region, labeled V_o, is given by equation 1. The volume of the third concentric ring, labeled V_3, is given by equation 2 with $n = 3$.

Figure 5. Total (integrated) calcium signal I(t) at various times after the start of calcium vaporization. I(t) is proportional to the number of free, vapor-phase calcium atoms in the vapor cloud at the time t after vaporization begins. The experimental data points are shown as triangles. When the experimental points taken during vaporization are fit to a linear approximation to vaporization (equation 6), equation 7 results. The solid curve is the result of this linear approximation.

Figure 6. Diffusion coefficient of calcium in an air-acetylene flame calculated at various times after the onset of vaporization. The diffusion coefficients were determined by fitting experimental data, such as shown in Figure 3, to equation 4. This equation incorporates the convolution of diffusion and vaporization to determine the function $C(r,t)$; a spherical Abel-type series relates $C(r,t)$ to the experimental signal observed. Since experimental and theoretical errors are relatively larger during vaporization than after it, the average of values after vaporization ($3.4\ cm^2/s$) reveals the true diffusion coefficient.

Figure 7. Integrated calcium signal $\underline{I(t)}$ in a nitrous oxide-acetylene flame from phosphate-free (□) and phosphate-containing (○) matrices. The experimental signals are proportional to the total number of free calcium atoms at a certain time after the beginning of vaporization. The droplets used were 65 μm in diameter and contained 100 μg Ca/mL as the chloride. The data represented by O's are for droplets containing 100 μg Ca/mL with a 0.5 PO_4/Ca molar ratio under otherwise identical experimental conditions. Both data sets were fitted to equation 6 and the resulting functions plotted as solid lines. Calcium from the phosphate-containing matrix volatilizes 30% more slowly than from a phosphate-free matrix.

Figure 8. Signals, $\underline{i(t)}$, from calcium vapor clouds in a nitrous oxide-acetylene flame. Aqueous droplets, identical in size and calcium content but one group free of phosphate and the other group containing a 0.5 PO_4/Ca molar ratio were injected into a laminar nitrous oxide-acetylene flame. The vapor clouds were observed 4 milliseconds after the start of analyte emission in each case and were found to contain approximately the same number of atoms (see Figure 7). Curve $\underline{A}$, the signal from the phosphate-containing matrix, is taller and narrower than curve $\underline{B}$, which is from the phosphate-free droplet. The shapes of these curves indicate that the phosphate-free droplet produced a more diffuse vapor cloud than the droplet containing phosphate.

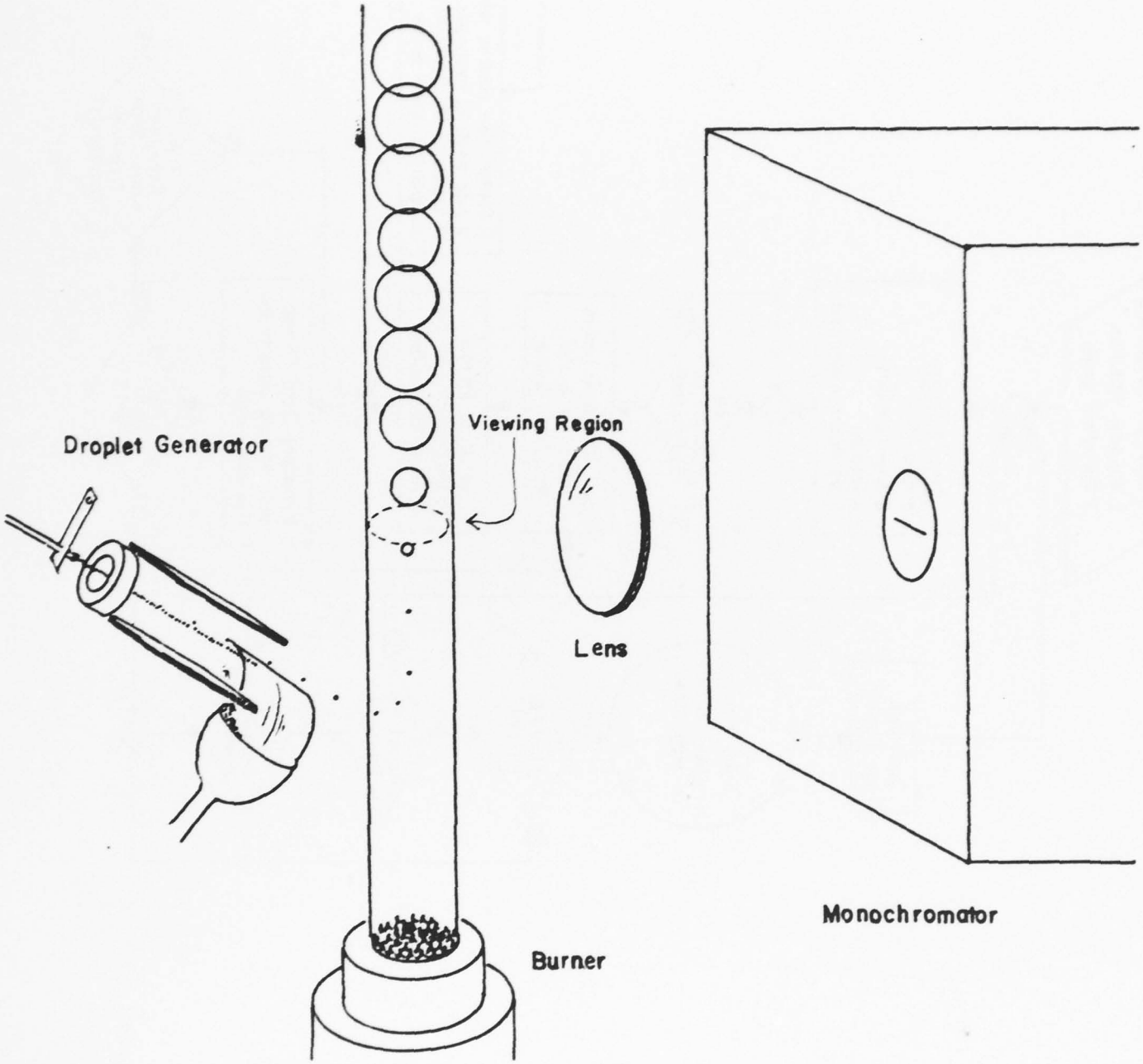
Droplet Generator
Viewing Region
Lens
Monochromator
Burner

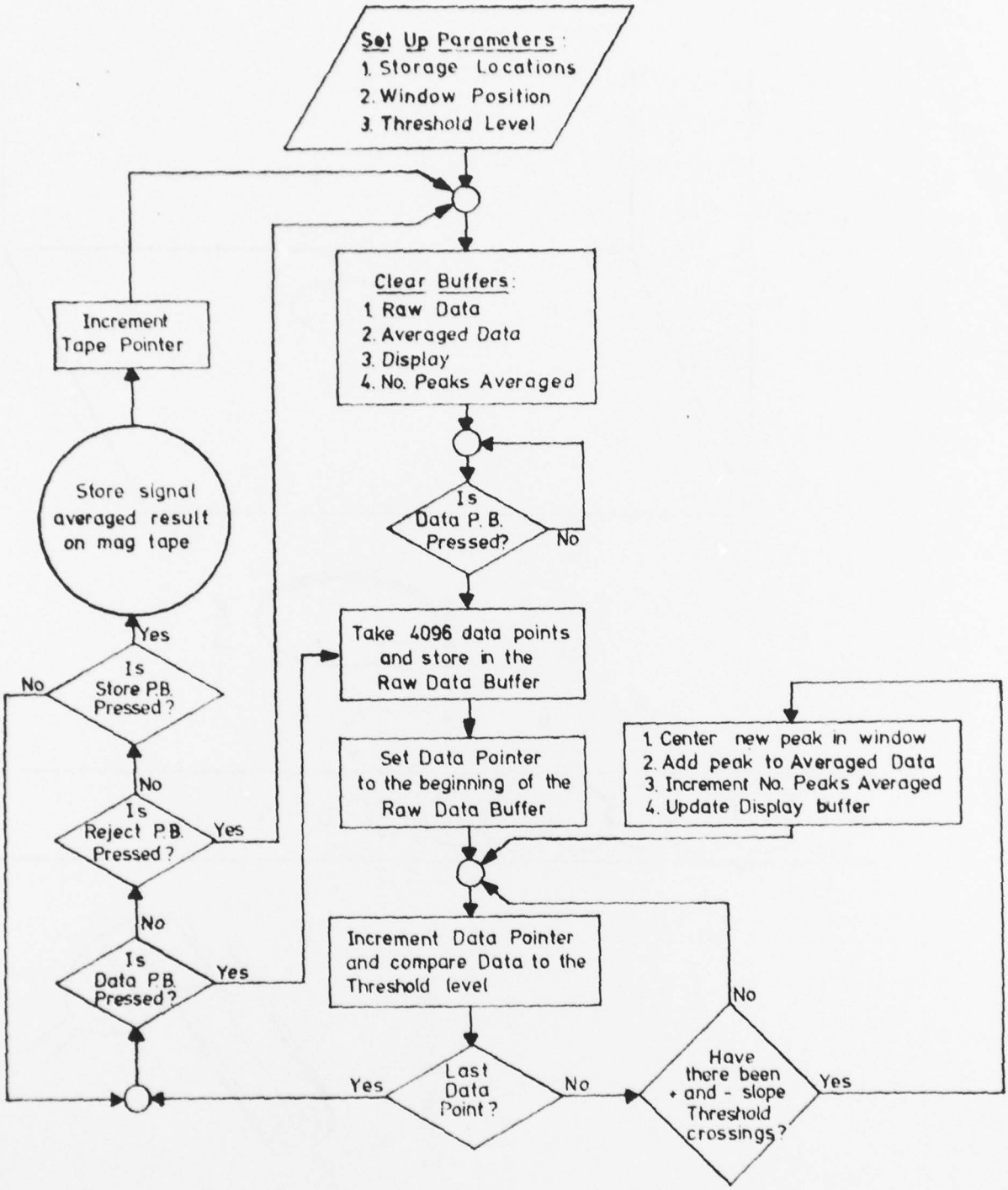
Set Up Parameters:
1. Storage Locations
2. Window Position
3. Threshold Level
Clear Buffers:
1. Raw Data
2. Averaged Data
3. Display
4. No. Peaks Averaged
Is Data P.B. Pressed?
No
Take 4096 data points and store in the Raw Data Buffer
Set Data Pointer to the beginning of the Raw Data Buffer
1. Center new peak in window
2. Add peak to Averaged Data
3. Increment No. Peaks Averaged
4. Update Display buffer
Increment Data Pointer and compare Data to the Threshold level
Last Data Point?
Yes
No
Have there been + and - slope Threshold crossings?
Yes
No
Is Data P.B. Pressed?
Yes
No
Is Reject P.B. Pressed?
Yes
No
Is Store P.B. Pressed?
Yes
No
Store signal averaged result on mag tape
Increment Tape Pointer

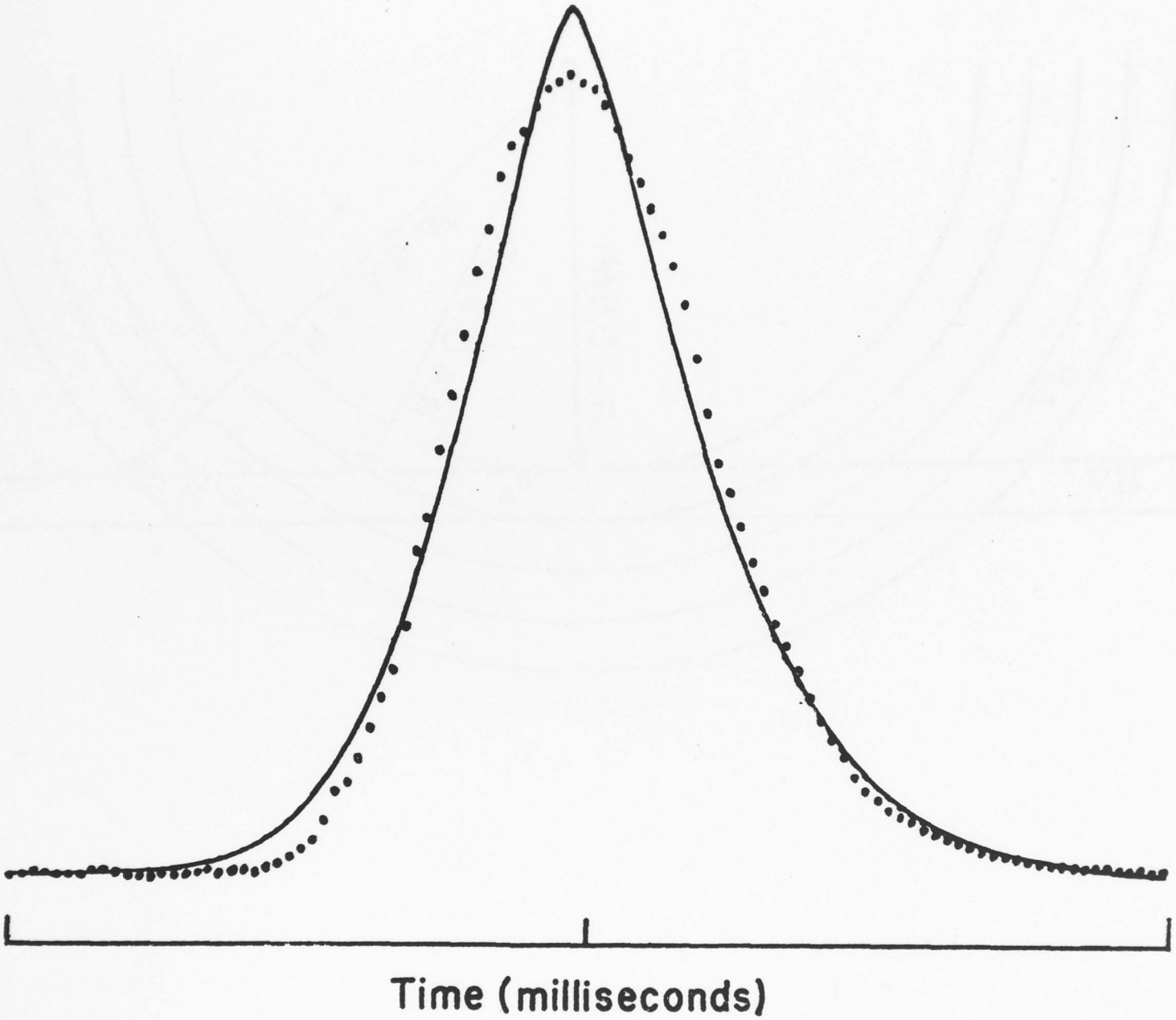
Time (milliseconds)

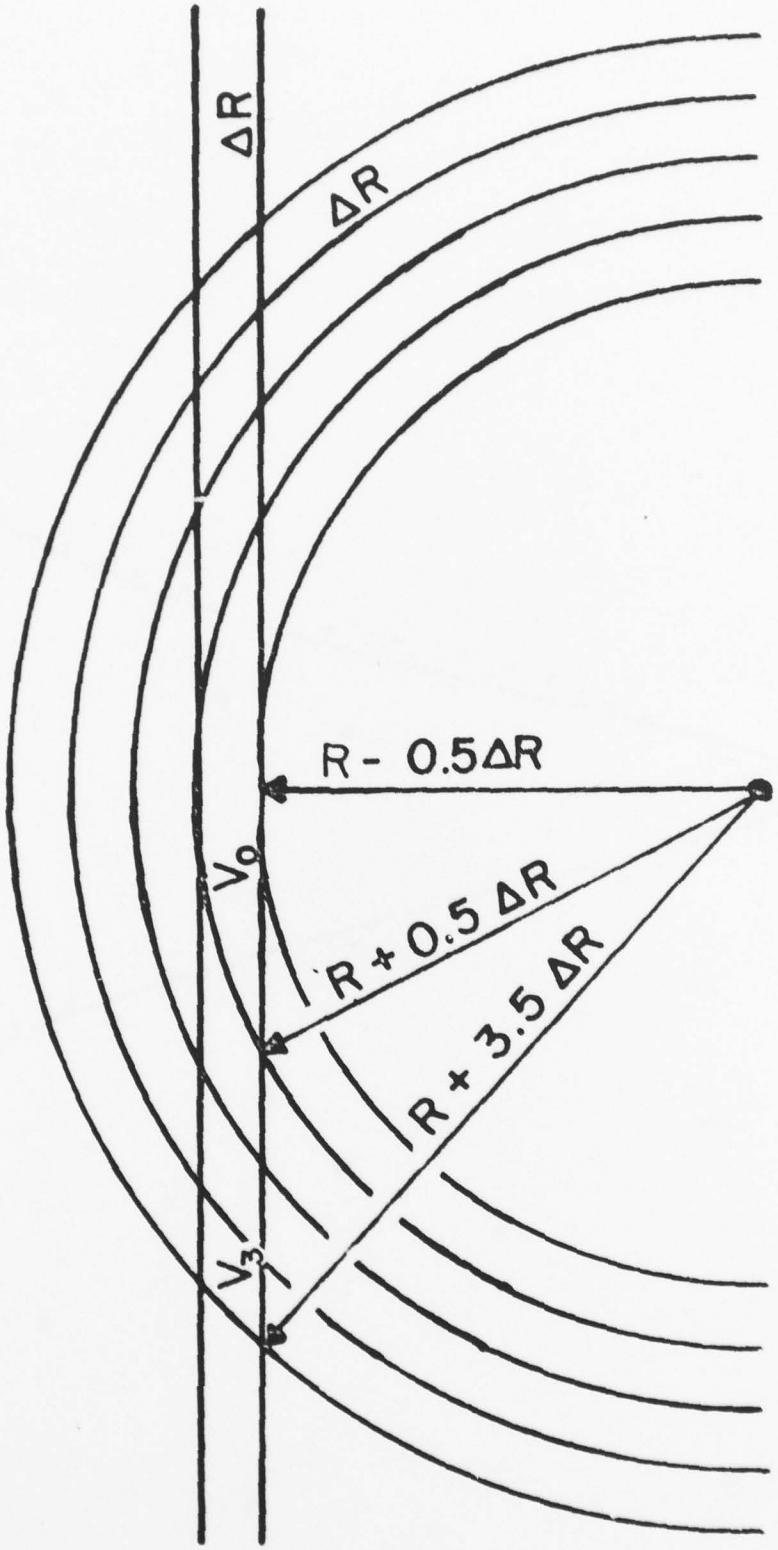
ΔR
ΔR
R - 0.5ΔR
V0
R + 0.5 ΔR
R + 3.5 ΔR
V3

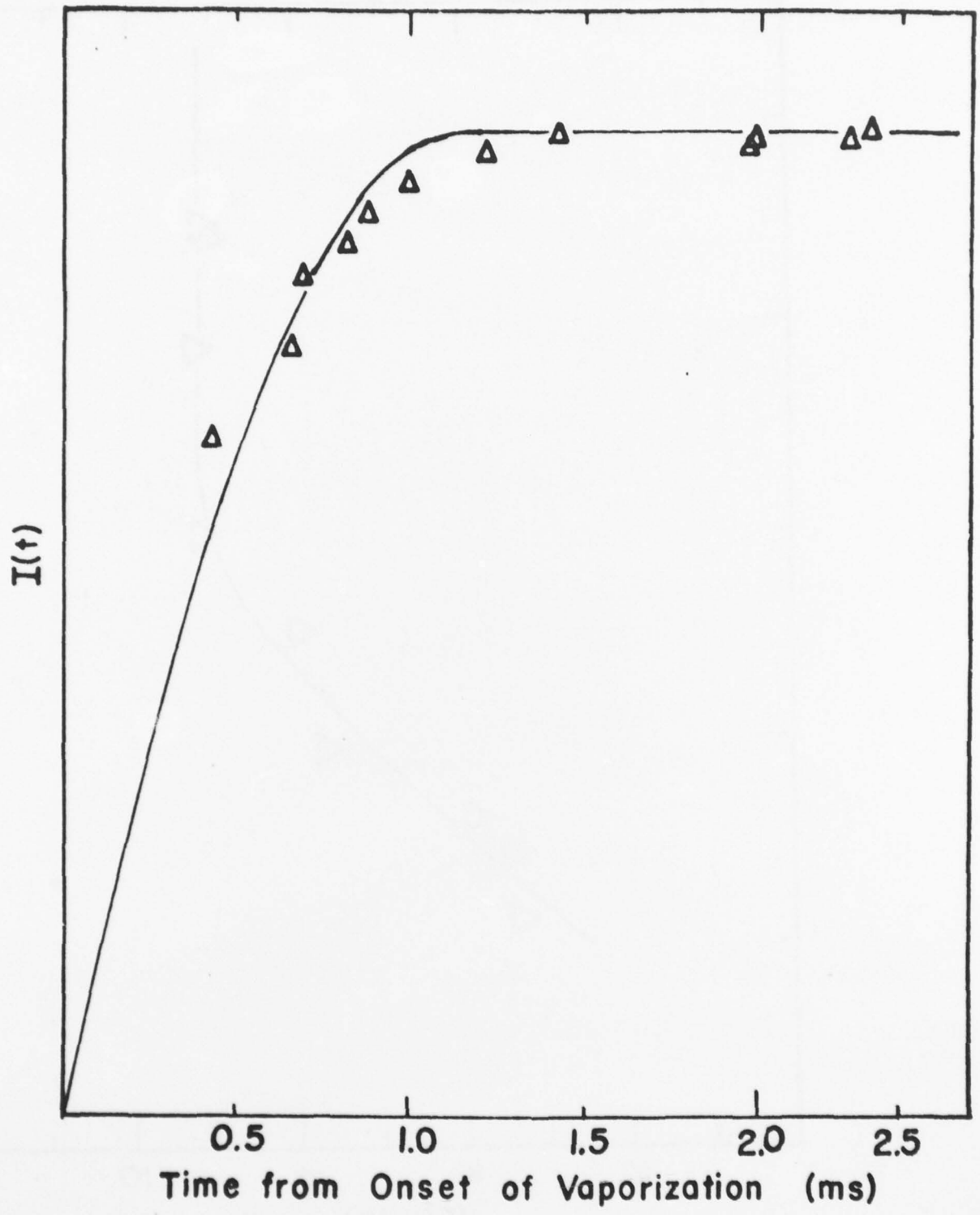
I(t)
0.5
1.0
1.5
2.0
2.5
Time from Onset of Vaporization (ms)

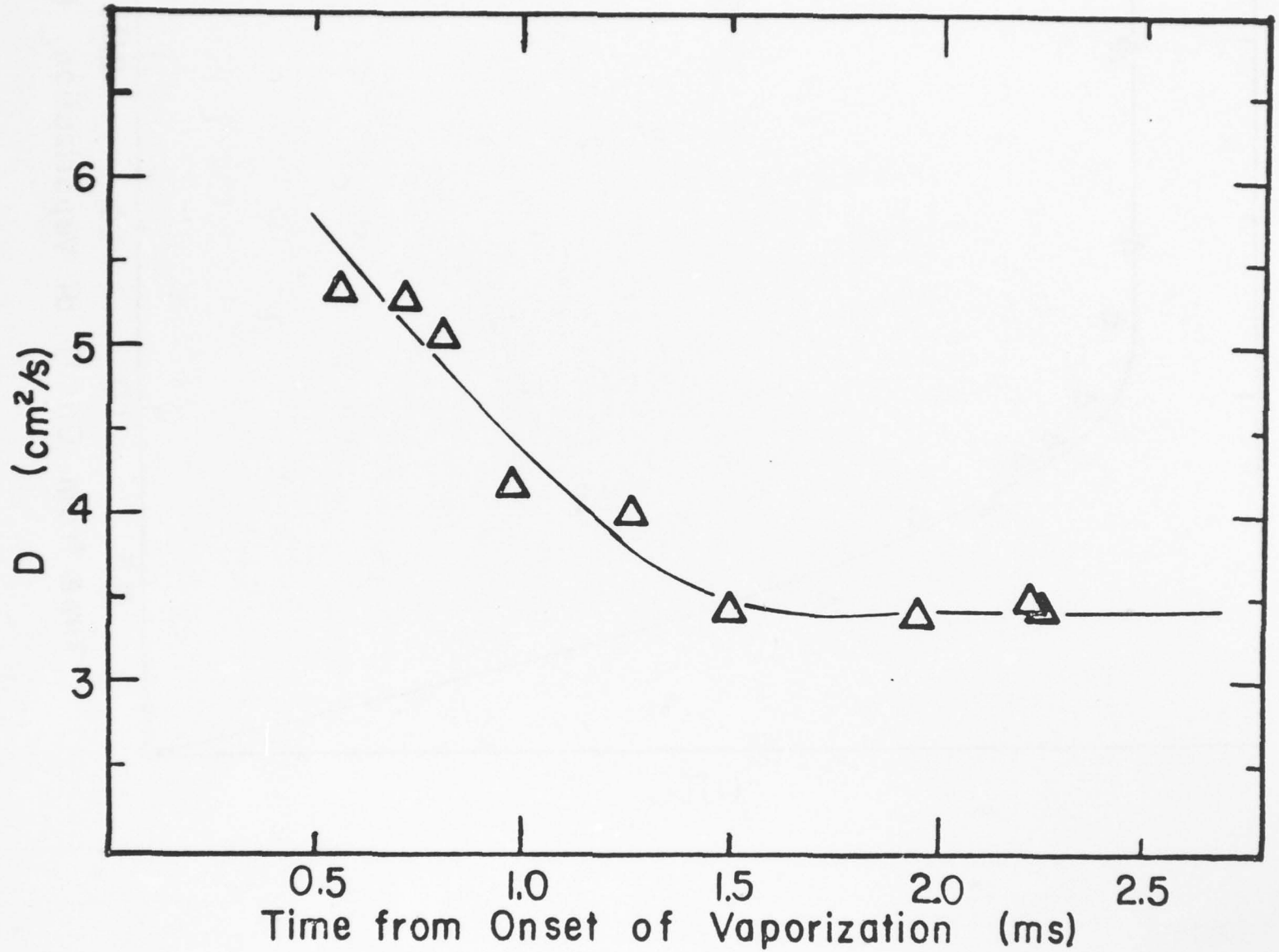
D (cm²/s)
6
5
4
3
0.5
1.0
1.5
2.0
2.5
Time from Onset of Vaporization (ms)

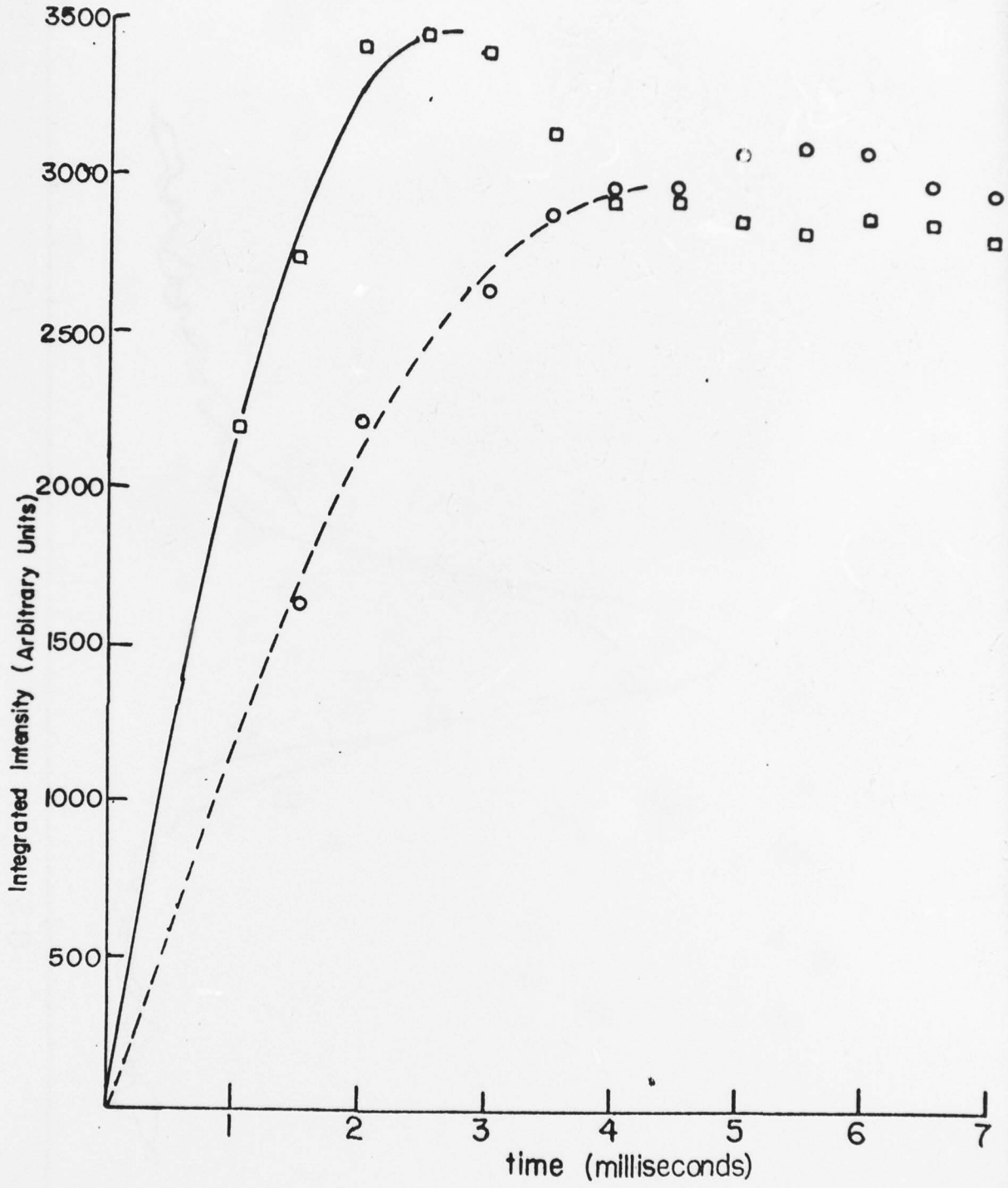
3500
3000
2500
2000
1500
1000
500
Integrated Intensity (Arbitrary Units)
1
2
3
4
5
6
7
time (milliseconds)

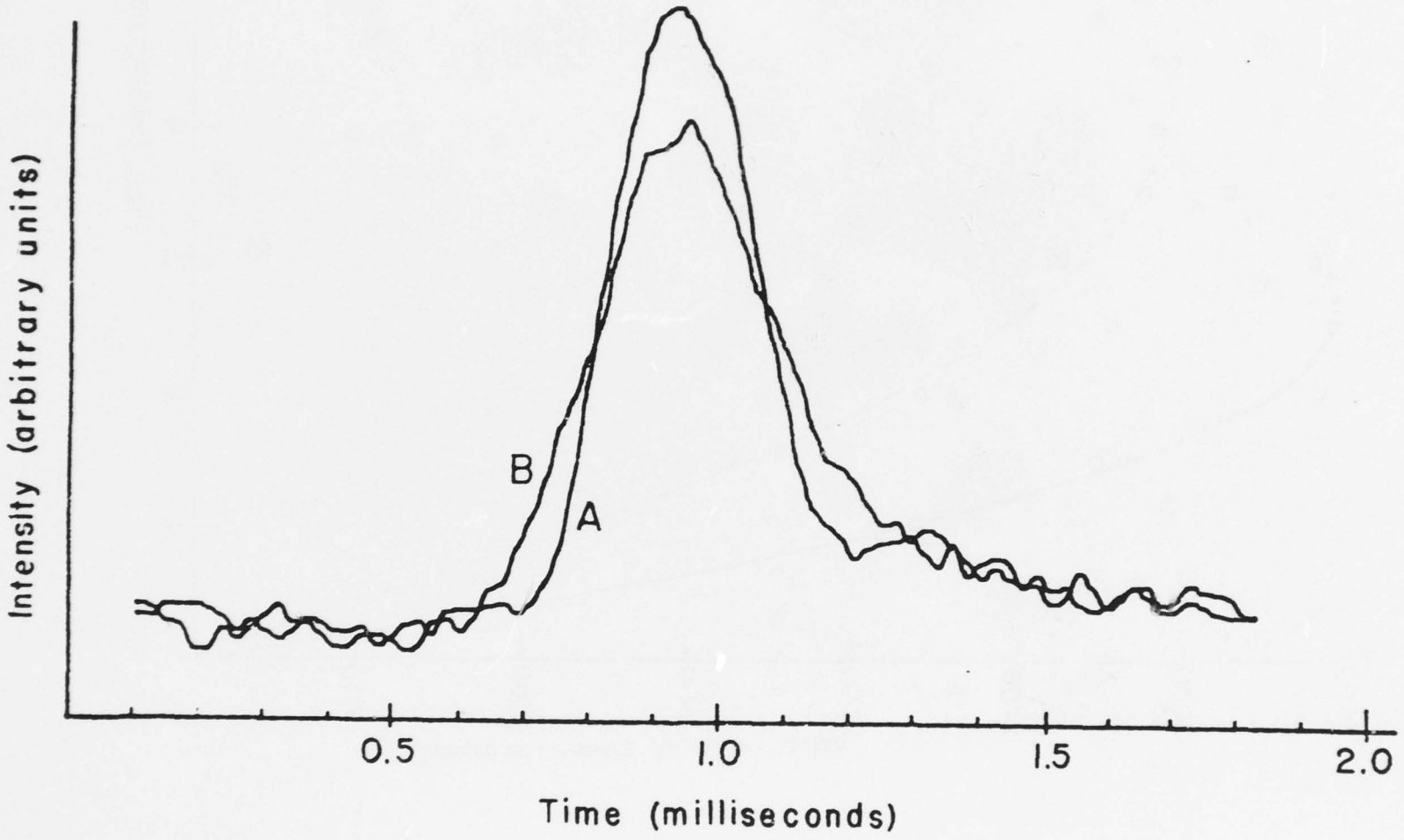
Intensity (arbitrary units)
B
A
0.5
1.0
1.5
2.0
Time (milliseconds)

472:GAN:716:t
78u472-608

TECHNICAL REPORT DISTRIBUTION LIST, GEN

	No. Copies
Office of Naval Research 800 North Quincy Street Arlington, Virginia 22217 Attn: Code 472	2
ONR Branch Office 536 S. Clark Street Chicago, Illinois 60605 Attn: Dr. George Sandoz	1
ONR Branch Office 715 Broadway New York, New York 10003 Attn: Scientific Dept.	1
ONR Branch Office 1030 East Green Street Pasadena, California 91106 Attn: Dr. R. J. Marcus	1
ONR Area Office One Hallidie Plaza, Suite 601 San Francisco, California 94102 Attn: Dr. P. A. Miller	1
ONR Branch Office Building 114, Section D 666 Summer Street Boston, Massachusetts 02210 Attn: Dr. L. H. Peebles	1
Director, Naval Research Laboratory Washington, D.C. 20390 Attn: Code 6100	1
The Assistant Secretary of the Navy (R,E&S) Department of the Navy Room 4E736, Pentagon Washington, D.C. 20350	1
Commander, Naval Air Systems Command Department of the Navy Washington, D.C. 20360 Attn: Code 310C (H. Rosenwasser)	1

	No. Cop
Defense Documentation Center Building 5, Cameron Station Alexandria, Virginia 22314	1
U.S. Army Research Office P.O. Box 1211 Research Triangle Park, N.C. 27709 Attn: CRD-AA-IP	
Naval Ocean Systems Center San Diego, California 92152 Attn: Mr. Joe McCartney	
Naval Weapons Center China Lake, California 93555 Attn: Dr. A. B. Amster Chemistry Division	
Naval Civil Engineering Laboratory Port Hueneme, California 93401 Attn: Dr. R. W. Drisko	
Professor K. E. Woehler Department of Physics & Chemistry Naval Postgraduate School Monterey, California 93940	
Dr. A. L. Slafkosky Scientific Advisor Commandant of the Marine Corps (Code RD-1) Washington, D.C. 20380	
Office of Naval Research 800 N. Quincy Street Arlington, Virginia 22217 Attn: Dr. Richard S. Miller	
Naval Ship Research and Development Center Annapolis, Maryland 21401 Attn: Dr. G. Bosmajian Applied Chemistry Division	
Naval Ocean Systems Center San Diego, California 91232 Attn: Dr. S. Yamamoto, Marine Sciences Division	

Encl 1

TECHNICAL REPORT DISTRIBUTION LIST, 051C

	No. Copies
Dr. M. B. Denton University of Arizona Department of Chemistry Tucson, Arizona 85721	1
Dr. R. A. Osteryoung Colorado State University Department of Chemistry Fort Collins, Colorado 80521	1
Dr. B. R. Kowalski University of Washington Department of Chemistry Seattle, Washington 98105	1
Dr. S. P. Perone Purdue University Department of Chemistry Lafayette, Indiana 47907	1
Dr. D. L. Venezky Naval Research Laboratory Code 6130 Washington, D.C. 20375	1
Dr. H. Freiser University of Arizona Department of Chemistry Tuscon, Arizona 85721	
Dr. Fred Saalfeld Naval Research Laboratory Code 6110 Washington, D.C. 20375	1
Dr. H. Chernoff Massachusetts Institute of Technology Department of Mathematics Cambridge, Massachusetts 02139	1
Dr. K. Wilson University of California, San Diego Department of Chemistry La Jolla, California 92037	1
Dr. A. Zirino Naval Undersea Center San Diego, California 92132	1
Dr. John Duffin United States Naval Postgraduate School Monterey, California 93940	1
Dr. G. M. Hieftje Department of Chemistry Indiana University Bloomington, Indiana 47401	1
Dr. Victor L. Rehn Naval Weapons Center Code 3813 China Lake, California 93555	1
Dr. Christie G. Enke Michigan State University Department of Chemistry East Lansing, Michigan 48824	1
Dr. Kent Eisentraut, MBT Air Force Materials Laboratory Wright-Patterson AFB, Ohio 45433	1
Walter G. Cox, Code 3632 Naval Underwater Systems Center Building 148 Newport, Rhode Island 02840	1